



Hydrothermal Fe cycling and deep ocean organic carbon scavenging: Model-based evidence for significant POC supply to seafloor sediments



C.R. German^{a,*}, L.L. Legendre^{b,c}, S.G. Sander^d, N. Niquil^e, G.W. Luther III^f, L. Bharati^g, X. Han^h, N. Le Brisⁱ

^a Woods Hole Oceanographic Institution, Woods Hole, MA 02543, USA

^b Sorbonnes Universités, UPMC Univ. Paris 06, LOV, Observatoire océanologique, 06230 Villefranche-sur-Mer, France

^c CNRS, LOV, Observatoire océanologique, 06230 Villefranche-sur-Mer, France

^d NIWA/University of Otago Research Centre for Oceanography, Department of Chemistry, University of Otago, New Zealand

^e CNRS, UMR 7208 BOREA, Laboratoire BioMea (FRE 3484), Université de Caen Basse-Normandie, 14032 Caen, France

^f School of Marine Science and Policy, College of Earth, Ocean and Environment, University of Delaware, DE 19716, USA

^g Microbiology Laboratory, National Institute of Oceanography, Dona Paula – 403 004, Goa, India

^h Second Institute of Oceanography, SOA, Hangzhou, Zhejiang 310012, China

ⁱ Sorbonne Universités, UPMC Univ Paris 06, Laboratoire d'Ecogéochimie des Environnements Benthiques (LECOB UMR 8222), Observatoire Océanologique, F-66650, Banyuls-sur-Mer, France

ARTICLE INFO

Article history:

Received 15 August 2014

Received in revised form 27 February 2015

Accepted 5 March 2015

Available online 30 March 2015

Editor: G.M. Henderson

Keywords:

hydrothermal venting

ocean biogeochemistry

iron

organic carbon

inverse model

ABSTRACT

Submarine hydrothermal venting has recently been identified to have the potential to impact ocean biogeochemistry at the global scale. This is the case because processes active in hydrothermal plumes are so vigorous that the residence time of the ocean, with respect to cycling through hydrothermal plumes, is comparable to that of deep ocean mixing caused by thermohaline circulation. Recently, it has been argued that seafloor venting may provide a significant source of bio-essential Fe to the oceans as the result of a close coupling between Fe and organic carbon in hydrothermal plumes. But a complementary question remains to be addressed: does this same intimate Fe–C_{org} association in hydrothermal plumes cause any related impact to the global C cycle? To address this, SCOR-InterRidge Working Group 135 developed a modeling approach to synthesize site-specific field data from the East Pacific Rise 9°50' N hydrothermal field, where the range of requisite data sets is most complete, and combine those inputs with global estimates for dissolved Fe inputs from venting to the oceans to establish a coherent model with which to investigate hydrothermal C_{org} cycling. The results place new constraints on submarine Fe vent fluxes worldwide, including an indication that the majority of Fe supplied to hydrothermal plumes should come from entrainment of diffuse flow. While this same entrainment is not predicted to enhance the supply of dissolved organic carbon to hydrothermal plumes by more than ~10% over background values, what the model does indicate is that scavenging of carbon in association with Fe-rich hydrothermal plume particles should play a significant role in the delivery of particulate organic carbon to deep ocean sediments, worldwide.

© 2015 Elsevier B.V. All rights reserved.

1. Introduction

Submarine hydrothermal venting was first discovered in the late 1970s (Corliss et al., 1978) and was almost immediately recognized as a potentially important source and sink of key elements in global-ocean geochemical budgets (Edmond et al., 1979).

With the discovery of the first high-temperature black smokers (Spiess et al., 1980), a further appreciation arose that the gross fluxes emitted from high-temperature venting were modified significantly in hydrothermal plumes. For the vast majority of chemical tracers enriched in vent fluids, net fluxes to the oceans are modified as these tracers are incorporated into Fe-rich polymetallic sulfide and oxyhydroxide particles that sink to the seafloor at and close to mid ocean ridge crests (Mottl and McConachy, 1990; German et al., 1991; Kadko, 1993). This view of the restricted role that hydrothermal systems might play in global-scale budgets persisted for more than a decade although, for those trace elements and isotopes that are readily scavenged by Fe, it was recognized

* Corresponding author. Tel.: +1 508 289 2853.

E-mail addresses: cgerman@whoi.edu (C.R. German), legendre@obs-vlfr.fr (L.L. Legendre), sylvia.sander@otago.ac.nz (S.G. Sander), nathalie.niquil@unicaen.fr (N. Niquil), luther@udel.edu (G.W. Luther), loka@nio.org (L. Bharati), xqhan@mail.hz.zj.cn (X. Han), lebris@obs-banyuls.fr (N. Le Bris).

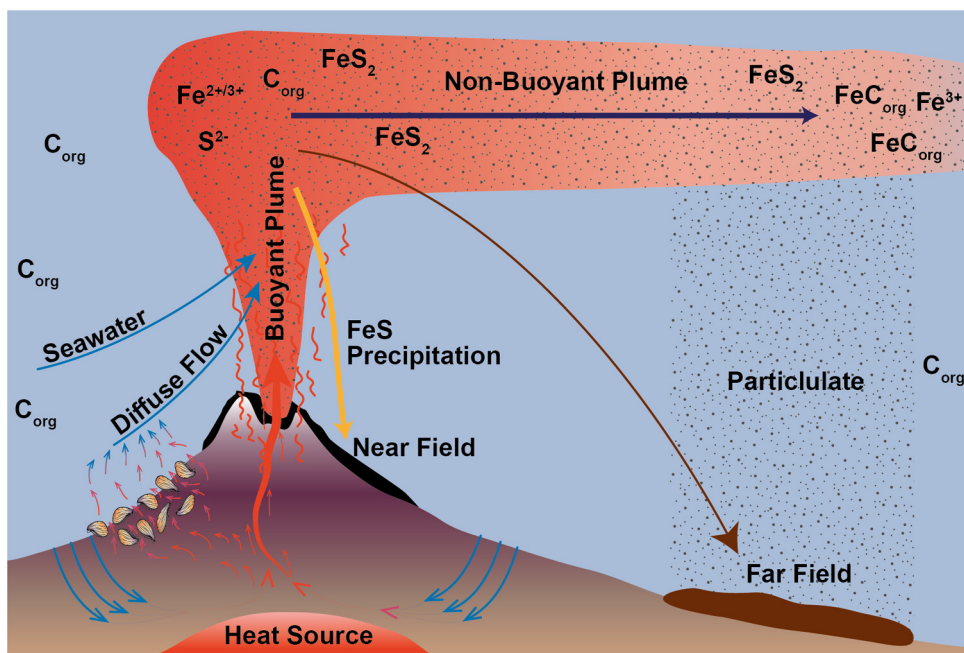


Fig. 1. Schematic of processes associated with submarine hydrothermal plumes showing the three sources of fluid inputs to buoyant hydrothermal plumes (focused vent flow, diffuse vent flow and entrained seawater). The buoyant plume continues to entrain background seawater progressively as it rises until a level of neutral buoyancy is attained. Extensive precipitation of some bulk phase polymetallic sulfides and other phases occurs during this plume rise and results in an important settling flux of material directly to the immediately adjacent seafloor. Much additional material is incorporated into the dispersing non-buoyant plume, however, and this provides an important mechanism for the export of dissolved and (nano-)particulate material away from ridge axes into the deep ocean interior.

that the net effect of submarine venting might be to remove dissolved trace elements and isotopes (TEIs) from the deep ocean into underlying sediments (Elderfield and Schultz, 1996). By contrast, until recently the potential impact of hydrothermal venting on the global carbon cycle was almost completely overlooked (cf. German and Von Damm, 2003; German and Seyfried, 2014).

1.1. Coupling of iron with organic carbon in deep-sea hydrothermal plumes

In the past decade, with the advent of the international GEO-TRACES program (www.geotraces.org), multiple high-quality basin-scale data sets have emerged that show that there is a significant component of dissolved Fe present in the deep ocean at dispersing hydrothermal plume depths (Wu et al., 2011; Klunder et al., 2011, 2012; Saito et al., 2013; Nishioka et al., 2013; Conway and John, 2014; Fitzsimmons et al., 2014; Sedwick et al., 2014; Hatta et al., in press; Resing et al., submitted for publication). Further, global-scale biogeochemical modeling appears to require such hydrothermal inputs to exist to reproduce the reported distributions of dissolved Fe globally (Tagliabue et al., 2010; Sedwick et al., 2014; Resing et al., submitted for publication). In parallel, near-field hydrothermal research has focused upon what mechanisms might prevent dissolved Fe from being removed into underlying sediments through oxidative precipitation and, hence, facilitate a dissolved Fe export flux from venting. To-date, two hypotheses have been put forward. The first suggests that dissolved Fe(II) and Fe(III) may be complexed by organic ligands that are also present within the turbulent plumes found directly above high-temperature vents and which mix diffuse flow and ambient seawater together with end-member vent fluids (Bennett et al., 2008; Sander and Koschinsky, 2011; Hawkes et al., 2013). Those studies have calculated that 0.1–7.5% of the gross dissolved Fe flux from hydrothermal venting could be stabilized by organic complexation. The second hypothesis, equally consistent with the available data, suggests that rather than being present in truly dissolved form, some of the Fe passing through operational filtration

processes may be present as nano-particulate pyrite (FeS_2). Their small size and kinetic stability against oxidation would allow these FeS_2 nanoparticles to travel farther than their larger analogs before undergoing oxidative dissolution, with any Fe(II) or (III) released being complexed by excess organic ligands (Yucel et al., 2011; Gartman et al., 2014). Either process could stabilize Fe sufficiently for iron from hydrothermal vent sources to be exported to the deep ocean interior.

Because Fe is an essential micronutrient limiting photosynthetically-driven productivity in up to 40% of the world's surface oceans, it is of great importance to better understand the sources and pathways of Fe in the ocean, particularly at a time when significant changes in the aerosol iron supply are expected, due to a more arid climate and increased dust precipitation (Boyd and Ellwood, 2010). In parallel, what has become increasingly apparent from hydrothermal process studies over the past decade, focused at the East Pacific Rise (EPR) 9°50' N vent field, is that the Fe cycle in hydrothermal plumes may be intimately linked to the cycling of organic carbon (Toner et al., 2009; Bennett et al., 2011; Breier et al., 2012). While detailed studies have provided important new insights into the processes active in hydrothermal plumes, however, such approaches do not allow for a quantitative consideration of their potential importance to global-scale biogeochemical budgets (German and Seyfried, 2014). Here, we have developed a modeling approach, constrained by the most complete set of bounding conditions available (from the EPR 9°50' N vent field), to address the key question:

- Do the processes that regulate dissolved and particulate Fe fluxes through submarine hydrothermal plumes also impact ocean cycling of organic carbon at the global scale?

1.2. Conceptual Model for investigating hydrothermal Fe & C_{org} cycling

Fig. 1 shows the conceptual framework for our study. While the role of microbes in the oxidation and reduction of iron in hydrothermal plumes and diffuse vents is well established as an important pathway for the coupling of Fe and organic C

(Emerson and Moyer, 2002; Dick et al., 2013; Li et al., 2014), our modeling approach does not need to distinguish between abiotic and biologically-driven processes to arrive at important conclusions concerning net Fe and organic C fluxes. Hydrothermal fluids emitted from high-temperature vents at the seafloor are initially hot (hence, buoyant) and strongly enriched in dissolved Fe (up to 1 million times higher than typical deep ocean concentrations). As these fluids rise, they entrain large volumes of deep-ocean seawater together with variable amounts of diffuse flow emitted from lower-temperature venting across the surrounding hydrothermal field. Both the diffuse flow and the surrounding seawater may be significant sources of organic carbon to the system (including in the form of iron-binding ligands) and the diffuse flow may also be a source of Fe, albeit at much lower concentrations than in high-temperature vent fluids (Luther et al., 2001; Koschinsky et al., 2002). Within the buoyant hydrothermal plume, vent fluids rapidly undergo progressive dilution until they are no longer buoyant and rise no further. Typical heights of rise associated with submarine hydrothermal plumes are of the order of 100 m or more and the time taken for emplacement at this non-buoyant plume height is of the order of 1 h during which the end-member vent fluids undergo dilutions of $\sim 10,000:1$ with background seawater and diffuse flow (Lupton, 1995). Processes that are most likely to influence the fate of Fe in buoyant hydrothermal plumes include: precipitation of bulk phase polymetallic sulfides as the vent fluids cool; complexation of dissolved Fe with organic ligands as the vent fluids mix with the entrained seawater and diffuse flow; and oxidative precipitation of dissolved Fe(II) as the sulfide-bearing and completely anoxic vent fluids mix with well-oxygenated entrained bottom water.

While precipitation of polymetallic sulfides is expected to be rapid with respect to the rise time of buoyant hydrothermal plumes (Rudnicki and Elderfield, 1993), Fe-oxidation rates vary progressively as oceanic deep water circulates progressively, from one ocean basin to the next, along the global thermohaline conveyor (Field and Sherrell, 2000; Statham et al., 2005). For the majority of deep ocean basins, significant concentrations of dissolved as well as particulate Fe should persist as far as the top of rising, buoyant hydrothermal plumes. Removal of Fe into particulate form may then proceed, with or without microbial mediation, as the resulting non-buoyant plumes are dispersed by deep ocean currents (Dick et al., 2013; German and Seyfried, 2014). Thus, we anticipate that the major removal processes for Fe into underlying sediments are in the forms of both polymetallic sulfides close to sites of active venting and Fe-oxyhydroxide phases settling out beneath dispersing non-buoyant plumes.

2. Methods: modeling Fe and organic carbon cycling in hydrothermal plumes

2.1. Model implementation using Fe as “currency”

Fig. 2 shows the processes outlined in the preceding section encapsulated into a model structure in which there are three types of Fe input into a buoyant hydrothermal plume (1: vent fluids; 2: entrained diffuse flow; and 3: entrained seawater) and three terms representing Fe removal (1.1: sedimentation from the buoyant plume as polymetallic sulfides; 4.1: sedimentation from the non-buoyant plume in particulate form; and 4.2: export to the deep ocean in dissolved [and nano-particulate] form). Note that there is one additional flow of Fe, Fe-Flow_{1,2}, that is not portrayed in Fig. 2. Fe-Flow_{1,2} is the fraction of Fe-Flow₁ that persists in solution and is incorporated into the non-buoyant plume, together with Fe-Flow₂ (diffuse flow) and Fe-Flow₃ (entrained seawater). All of Fe-Flow_{1,2}, Fe-Flow₂, and Fe-Flow₃, are carried away from the vent source as Fe-Flow₄.

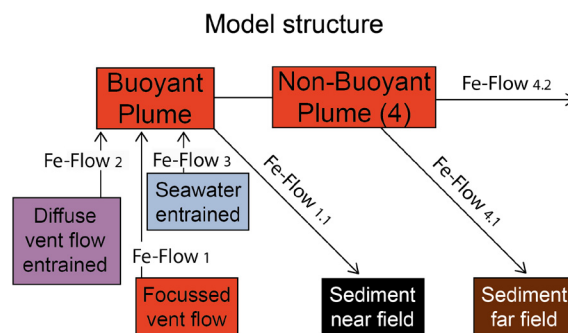


Fig. 2. Structure of the SCOR-InterRidge WG135 model for biogeochemical cycling in deep sea hydrothermal plumes using Fe as “currency”. This figure translates the processes illustrated in Fig. 1 into a series of key flows (labeled arrows) that form the basis of the model: Fe-Flow₁, Fe-Flow₂ and Fe-Flow₃ represent the three primary inputs to buoyant hydrothermal plumes from focused vent flow (Fe-Flow₁), diffuse hydrothermal flow (Fe-Flow₂) and entrained seawater (Fe-Flow₃), respectively. Fe-Flow₁ is subdivided into Fe-Flow_{1,1} and Fe-Flow_{1,2}. Fe-Flow_{1,1} represents the removal flux associated with the rapid precipitation of particulate phases in buoyant hydrothermal plumes, immediately above a vent site, that settle to the immediately adjacent seafloor. Fe-Flow_{1,2} (not shown) represents the remainder of Fe-Flow₁ which, together with Fe-Flow₂ and Fe-Flow₃ is incorporated into the dispersing hydrothermal plume as Fe-Flow₄. In turn, Fe-Flow₄ is partitioned into Fe-Flow_{4,1} and Fe-Flow_{4,2}. Fe-Flow_{4,1} represents the flux associated with particulate material that settles to deep ocean sediments beneath dispersing hydrothermal plumes while Fe-Flow_{4,2} represents the export flux of dissolved (\pm nano-particulate) iron that is dispersed into the deep ocean interior.

All units, values, expressions, and literature sources for the parameterization of our model are provided in Table 1. An important assumption that we have relied upon in constructing this model is that all hydrothermal systems, globally, can be represented by the circumstances that prevail at the EPR 9°50' N hydrothermal field. We note that the validity of this assumption is limited because: (i) vent fluid compositions vary along the global ridge crest, especially with changing lithologies such as those found at slow and ultraslow ridges and in back-arc settings; (ii) Fe reaction kinetics in hydrothermal plumes vary progressively along the global thermohaline conveyor (German and Seyfried, 2014). Nevertheless, following this approach achieves two important goals: (a) we are able, for the first time, to assemble various discrete data sets, acquired independently and over decades of field work, into a coherent framework, and (b) we are able to obtain model results, for both Fe and C cycling in hydrothermal systems, that are consistent with recent field observations (see later).

2.2. Derivation of the flow equations used in the model

In this section, we describe how the (mass-based) Fe-Flow equations used in the model were derived. A first key parameter (not illustrated in Fig. 2) is the Heat Flow Ratio, which defines the proportion of axial heat flux that is provided by focused hydrothermal fluid flow (Heat-Flow₁) or diffuse hydrothermal fluxes (Heat-Flow₂) across the seafloor/ocean interface. In our parameterization, we use the definition: $HFR = \text{Heat-Flow}_1 / (\text{Heat-Flow}_1 + \text{Heat-Flow}_2)$ and while the HFR value has no impact on the total hydrothermal heat flux at mid ocean ridges (2.6×10^{12} W), it significantly impacts the influence of hydrothermal venting upon ocean biogeochemistry, as reflected in our model results (see later). Accordingly, we have run our model with multiple HFR settings across the range 0.1–0.5 to accommodate the full spectrum of values considered plausible for seafloor hydrothermal systems (Table 1). In the remainder of this section, each Fe-Flow_x is represented by three successive equation types: conceptual (Cx), parameterized (Px), and as used in the numerical model (Mx). In Subsections 2.2.1 to 2.2.5, we detail the computation of the Fe-Flows in Fig. 2 assuming that the value of the flow of Fe that

Table 1
Parameters used for SCOR-InterRidge WG 135 Hydrothermal Fe-C_{org} cycling model.

Parameter	Units	Value or expression	Literature source and comments
Fe molar mass	kg mol ⁻¹	55.845 × 10 ⁻³	–
Heat Flow Ratio (HFR)	Dimensionless	0.1 to 0.5	Estimated range of HFR (Elderfield and Schultz, 1996; Mottl, 2003).
Total Heat Flow	W	2.6 × 10 ¹²	Global heat flow anomaly in oceanic crust younger than 1 Ma attributed to on-axis hydrothermal flux of seawater heated beneath the seafloor to temperatures of 350–400 °C (Elderfield and Schultz, 1996).
Water-Flow ₁	kg yr ⁻¹	7.2 × 10 ¹² × (HFR/0.2)	Preferred value for hydrothermal water flux from fluids exiting the seafloor at black smoker (~350 °C) temperatures at HFR = 0.2 (Nielsen et al., 2006), multiplied by (HFR/0.2) to allow a range of HFR values to be considered.
(Water-Flow/Heat-Flow) ₂	kg yr ⁻¹ per W	3250	Flank flux calculation from Mottl (2003): 6.16 TW carried by 2 × 10 ¹⁹ g yr ⁻¹ ‘unaltered’ seawater @ 10 °C yields 3250 kg yr ⁻¹ per W.
Water-Flow ₃	kg yr ⁻¹	Water Flow ₁ × 10 ⁴ – Water Flow ₂	Assumes 10,000:1 dilution of high-temperature fluids (Lupton, 1995), includes all diffuse flow with remainder of volume flux provided by ambient seawater.
Fe concentration in Flow ₁ , [Fe] ₁	mol kg ⁻¹	2.5 × 10 ⁻³	Based on [Fe] vent-fluid data from EPR 9°50′ N (Bennett et al., 2011); Range: 0.85–4.1 mM, Ave: 2.5 mM.
Fe concentration in Flow ₂ , [Fe] ₂ ^a	mol kg ⁻¹	0.56 × 10 ⁻⁹	Minimum possible value, based on Fe concentration in ambient seawater (Wu et al., 2011).
Fe concentration in Flow ₃ , [Fe] ₃	mol kg ⁻¹	0.56 × 10 ⁻⁹	Fe concentration in ambient seawater (Wu et al., 2011).
k, fraction of Fe-Flow ₁ entering Fe-Flow _{1,1}	Dimensionless	0.5	As estimated by Rudnicki and Elderfield (1993).

^a Treated as a variable during later deterministic inverse model runs, leading to predicted [Fe]₂ values in the range: 7–965 μmol kg⁻¹ (see Section 3.3 and Table 3).

is incorporated into the non-buoyant plume (Fe-Flow₄) depends solely on the values of HFR and the parameters in the model. This type of computation is called *direct modeling*. In Subsections 2.2.6 to 2.2.8, we set the value of Fe-Flow₄ *a priori*, instead, and back-calculate the values of one parameter, [Fe]₂, as well as all other flows in the model that are impacted by setting the Fe-Flow₄ value. This second type of computation is referred to as *inverse modeling*.

2.2.1. Direct modeling of Fe-Flow₁

Conceptually:

$$\text{Fe-Flow}_1 = \text{Fe molar mass} \times [\text{Fe}]_1 \times \text{Water-Flow}_1 \quad (C1)$$

Eq. (C1) was parameterized using: Fe molar mass = 55.845 × 10⁻³, [Fe]₁ = 2.5 × 10⁻³, and Water-Flow₁ = (7.2 × 10¹²) × (HFR/0.2). Hence:

$$\text{Fe-Flow}_1 = (55.845 \times 10^{-3}) \times (2.5 \times 10^{-3}) \times (7.2 \times 10^{12}) \times (\text{HFR}/0.2) \quad (P1)$$

Combining the terms in Eq. (P1) provided the model equation for Fe-Flow₁, expressed as a function of HFR:

$$\text{Fe-Flow}_1 = 5,026,050,000 \times \text{HFR} \quad (M1)$$

2.2.1.1. Direct modeling of Fe-Flow_{1,1}

$$\text{Fe-Flow}_{1,1} = k \times \text{Fe-Flow}_1 \quad (C1.1)$$

Eq. (C1.1) was parameterized using: k = 0.5, i.e. half of Fe-Flow₁ is removed by Fe precipitation and sinking from the buoyant plume, in the near-field. Hence:

$$\text{Fe-Flow}_{1,1} = 0.5 \times \text{Fe-Flow}_1 \quad (P1.1)$$

The model equation for Fe-Flow_{1,1} was provided by Eq. (P1.1) and expressed as a function of Fe-Flow₁ (see Eq. (M1)):

$$\text{Fe-Flow}_{1,1} = 0.5 \times \text{Fe-Flow}_1 \quad (M1.1)$$

2.2.1.2. Direct modeling of Fe-Flow_{1,2}

$$\text{Fe-Flow}_{1,2} = \text{Fe-Flow}_1 - \text{Fe-Flow}_{1,1} \quad (C1.2)$$

The parameterized equation for model Fe-Flow_{1,2} was the same as Eq. (C1.2):

$$\text{Fe-Flow}_{1,2} = \text{Fe-Flow}_1 - \text{Fe-Flow}_{1,1} \quad (P1.2)$$

Fe-Flow_{1,2} was computed as a function of Fe-Flow₁ and Fe-Flow_{1,1} (Eqs. (M1) and (M1.1)):

$$\text{Fe-Flow}_{1,2} = \text{Fe-Flow}_1 - \text{Fe-Flow}_{1,1} \quad (M1.2)$$

2.2.2. Direct modeling of Fe-Flow₂

$$\text{Fe-Flow}_2 = \text{Fe molar mass} \times [\text{Fe}]_2 \times \text{Water-Flow}_2 \quad (C2)$$

Eq. (C2) was parameterized using: Fe molar mass = 55.845 × 10⁻³, [Fe]₂ = 5.6 × 10⁻¹⁰, and Water-Flow₂ = Heat-Flow₂ × (Water-Flow/Heat-Flow)₂, where (Water-Flow/Heat-Flow)₂ = 3250 kg yr⁻¹ W⁻¹ (Table 1). Hence:

$$\text{Fe-Flow}_2 = (55.845 \times 10^{-3}) \times (5.6 \times 10^{-10}) \times (\text{Heat-Flow}_2 \times 3250)$$

The value of HFR determines the partitioning of the total heat flow (2.6 × 10¹² W, Table 1) between focused and diffuse heat flow (Heat-Flow₁ & Heat-Flow₂, respectively):

$$\text{Heat-Flow}_1 = 2.6 \times 10^{12} \times \text{HFR}$$

$$\text{Heat-Flow}_2 = 2.6 \times 10^{12} \times (1 - \text{HFR})$$

Hence we obtained the parameterized equation for Fe-Flow₂:

$$\text{Fe-Flow}_2 = (55.845 \times 10^{-3}) \times (5.6 \times 10^{-10}) \times [2.6 \times 10^{12} \times (1 - \text{HFR})] \times 325 \quad (P2)$$

Substituting for HFR in Eq. (P2) using: HFR = Fe-Flow₁/5,026,050,000 (from Eq. (M1), above) we obtained the model equation for Fe-Flow₂, expressed as a function of Fe-Flow₁:

$$\text{Fe-Flow}_2 = 5.2577778 \times 10^{-5} \times (5,026,050,000 - \text{Fe-Flow}_1) \quad (M2)$$

2.2.3. Direct modeling of Fe-Flow₃

$$\text{Fe-Flow}_3 = \text{Fe molar mass} \times [\text{Fe}]_3 \times \text{Water-Flow}_3 \quad (C3)$$

Eq. (C3) was parameterized using: Fe molar mass = 55.845 × 10⁻³, [Fe]₃ = 5.6 × 10⁻¹⁰, and Water-Flow₃ = (Water-Flow₁ × 10⁴) – Water-Flow₂. Hence:

$$\text{Fe-Flow}_3 = (55.845 \times 10^{-3}) \times (5.6 \times 10^{-10}) \times [(\text{Water-Flow}_1 \times 10^4) - \text{Water-Flow}_2] \quad (P3)$$

But, from the equations for Fe-Flow₁ (Eqs. (C1) and (P1)) and Fe-Flow₂ (Eqs. (C2) and (P2)), we could also derive the expressions:

$$\text{Water-Flow}_1 \times 10^4 = \text{Fe-Flow}_1 / [(55.845 \times 10^{-3}) \times (2.5 \times 10^{-3}) \times (1 \times 10^{-4})]$$

$$\text{Water-Flow}_2 = \text{Fe-Flow}_2 / [(55.845 \times 10^{-3}) \times (5.6 \times 10^{-10})]$$

Substituting these expressions into Eq. (P3) we obtained the model equation:

$$\text{Fe-Flow}_3 = (0.00224 \times \text{Fe-Flow}_1) - \text{Fe-Flow}_2 \quad (M3)$$

2.2.4. Direct modeling of Fe-Flow₄

$$\text{Fe-Flow}_4 = \text{Fe-Flow}_{1,2} + \text{Fe-Flow}_2 + \text{Fe-Flow}_3 \quad (C4)$$

The parameterized and model equations for Fe-Flow₄ were the same as Eq. (C4):

$$\text{Fe-Flow}_4 = \text{Fe-Flow}_{1,2} + \text{Fe-Flow}_2 + \text{Fe-Flow}_3 \quad (P4)$$

$$\text{Fe-Flow}_4 = \text{Fe-Flow}_{1,2} + \text{Fe-Flow}_2 + \text{Fe-Flow}_3 \quad (M4)$$

All values of Fe Flow_{1,2}, Fe-Flow₂ and Fe-Flow₃ were computed using Eqs. (M1.2), (M2) and (M3), respectively.

2.2.5. Direct modeling of Fe-Flow_{4,1} and Fe Flow_{4,2}

Fe-Flow₄ was partitioned between Fe-Flow_{4,1} and Fe-Flow_{4,2} as follows:

$$\text{Fe-Flow}_{4,1} + \text{Fe-Flow}_{4,2} = \text{Fe-Flow}_4 \quad (C5)$$

$$\text{Fe-Flow}_{4,1} + \text{Fe-Flow}_{4,2} = \text{Fe-Flow}_4 \quad (P5)$$

$$\text{Fe-Flow}_{4,1} + \text{Fe-Flow}_{4,2} = \text{Fe-Flow}_4 \quad (M5)$$

2.2.6. Inverse modeling of [Fe]₂

For the inverse modeling runs, the value of Fe-Flow₄ was set to 231,200,000 kg Fe yr⁻¹ × c for the global ocean, using Fe-Flow_{4,2} = 231,200,000 kg Fe yr⁻¹ (Sedwick et al., 2014; Resing et al., submitted for publication) and c = [Fe-Flow₄/Fe-Flow_{4,2}]. The expression for [Fe]₂ was then derived from Eqs. (C2), (C3) and (C4) (above) in which:

$$[\text{Fe}]_2 = \text{Fe-Flow}_2 / (\text{Fe molar mass} \times \text{Water-Flow}_2) \text{ (from Eq. (C2))}$$

$$\text{Fe-Flow}_3 = \text{Fe molar mass} \times [\text{Fe}]_3 \times \text{Water-Flow}_3 \text{ (from Eq. (C3))}$$

$$\text{Fe-Flow}_2 = \text{Fe-Flow}_4 - (\text{Fe-Flow}_{1,2} + \text{Fe-Flow}_3) \text{ (from Eq. (C4))}$$

Hence:

$$[\text{Fe}]_2 = [(\text{Fe-Flow}_{4,2} \times c) - \{\text{Fe-Flow}_{1,2} + (\text{Fe molar mass} \times [\text{Fe}]_3 \times \text{Water-Flow}_3)\}] / (\text{Fe molar mass} \times \text{Water-Flow}_2) \quad (C6)$$

Expressions for each of these Water-Flow terms were obtained by combining expressions and parameters given previously in Sections 2.2.1–2.2.3 as follows:

$$- \text{Water-Flow}_1 = (7.2 \times 10^{12}) \times (\text{HFR}/0.2)$$

$$- \text{Water-Flow}_2 = 2.6 \times 10^{12} \times (1 - \text{HFR}) \times 3250$$

$$- \text{Water-Flow}_3 = (\text{Water-Flow}_1 \times 10^4) - \text{Water-Flow}_2$$

Then, substituting for (Water-Flow₁) and (Water-Flow₂), we obtained:

$$\text{Water-Flow}_3 = [(3684.5 \times \text{HFR}) - 84.5] \times 10^{14}$$

Combining this expression with Eqs. (P2), (P3) and (C6) yielded:

$$[\text{Fe}]_2 = (231,200,000 \times c) - \{\text{Fe-Flow}_{1,2} + (55.845 \times 10^{-3}) \times (5.6 \times 10^{-10}) \times [(3684.5 \times \text{HFR}) - 84.5] \times 10^{14}\} / [(55.845 \times 10^{-3}) \times 2.6 \times 10^{12} \times (1 - \text{HFR}) \times 3250] \quad (P6)$$

Hence, with Fe-Flow_{1,2} calculated from Eqs. (M1), (M1.1) and (M1.2), we obtained the model equation:

$$[\text{Fe}]_2 = \{(231,200,000 \times c) - [\text{Fe-Flow}_{1,2} + 3127.32 \times ((3684.5 \times \text{HFR}) - 84.5)]\} / [4718.9025 \times (1 - \text{HFR}) \times 10^{11}] \quad (M6)$$

2.2.7. Inverse modeling of Fe-Flow₂

In our inverse modeling, Eq. (C2) was used to provide an expression for Fe-Flow₂:

$$\text{Fe-Flow}_2 = \text{Fe molar mass} \times [\text{Fe}]_2 \times \text{Water-Flow}_2 \quad (C7)$$

This equation was then parameterized using expressions and parameters given in Section 2.2.2 above, with [Fe]₂ being computed using Eq. (M6), as follows:

$$\text{Fe-Flow}_2 = (55.845 \times 10^{-3}) \times [\text{Fe}]_2 \times [2.6 \times (1 - \text{HFR})] \times 32.5 \times 10^{14} \quad (P7)$$

This led directly to the model equation:

$$\text{Fe-Flow}_2 = 4718.9025 \times 10^{11} \times (1 - \text{HFR}) \times [\text{Fe}]_2 \quad (M7)$$

2.2.8. Inverse modeling of Fe-Flow₃

For inverse modeling runs, the expression for Fe-Flow₃ was obtained by difference between flows:

$$\text{Fe-Flow}_3 = \text{Fe-Flow}_4 - (\text{Fe-Flow}_{1,2} + \text{Fe-Flow}_2) \quad (C8)$$

where the value of Fe-Flow₄ was set to 231,200,000 × c, with c = [Fe-Flow₄/Fe-Flow_{4,2}] (see Section 2.2.6), and Fe-Flow_{1,2} and Fe-Flow₂ were estimated using Eqs. (M1.2) and (M7), respectively. The parameterized and model versions of the equation for Fe-Flow₃ were identical to Eq. (C8):

$$\text{Fe-Flow}_3 = \text{Fe-Flow}_4 - (\text{Fe-Flow}_{1,2} + \text{Fe-Flow}_2) \quad (P8)$$

$$\text{Fe-Flow}_3 = \text{Fe-Flow}_4 - (\text{Fe-Flow}_{1,2} + \text{Fe-Flow}_2) \quad (M8)$$

3. Model results

3.1. Fe cycling, linear inverse approach

The values of two key ratios in our model, the Heat Flux Ratio (HFR) and that for $[\text{Fe-Flow}_{4,2}/\text{Fe-Flow}_4]$ have each been debated extensively in the literature. For HFR, it has been argued that high-temperature focused flow may represent anything between 10% and 50% of the total axial heat flux and may vary according to geologic setting and/or spreading rate (Elderfield and Schultz, 1996; Mottl, 2003; German and Seyfried, 2014). When considering heat-flow at Mid Ocean Ridges, the differences associated with varying HFR are negligible but, by contrast, the potential differences for biogeochemical fluxes, according to any variation in the partitioning between heat transported in the form of metal-rich black smoker vent fluids vs. lower temperature (and typically metal depleted) diffuse flow are potentially profound. Historically, however, most attention has been paid to the geochemical characterization of high-temperature vent fluids, which provide important insights to the fluid–rock interaction processes occurring at depth beneath the seafloor. By contrast, much less attention has been paid to the characterization or quantification of diffuse-flow fluxes, precluding selection of a robust, globally representative “average” value for HFR. Accordingly, our approach throughout this study has been to calculate all possible model outcomes, across a wide range of HFR values, rather than rely upon a single HFR value with associated, poorly constrained, uncertainties (i.e. “errors”). Importantly, despite this relatively lightly constrained approach, our model results reveal important and robust outcomes from which our conclusions are drawn.

For the case of the ratio $[\text{Fe-Flow}_{4,2}/\text{Fe-Flow}_4]$, the flux of dissolved Fe from hydrothermal venting to the oceans ($\text{Fe-Flow}_{4,2}$) had been considered negligible by most researchers until the advent of the GEOTRACES program (Elderfield and Schultz, 1996; German and Seyfried, 2014). While work continues to better constrain the value of $[\text{Fe-Flow}_{4,2}/\text{Fe-Flow}_4]$, an early study by Sander and Koschinsky (2011) developed a geochemical model that considered end-member vent fluid data from the Turtle Pits and Rainbow fields on the Mid-Atlantic Ridge and calculated that ~0.10% to 0.33% of the dissolved hydrothermal iron released from those sites should stay in solution long enough to disperse away from the vent source.

To better estimate the values of the ratios HFR and $[\text{Fe-Flow}_{4,2}/\text{Fe-Flow}_4]$, we initially ran model Eqs. (M1)–(M5) (Section 2.2) using a linear inverse approach, which allows optimal solutions to be computed in those cases where the values of several flows are unknown (Vézina and Platt, 1988; Niquil et al., 2012). To obtain a numerical solution, the possible values of the unknown ratios had to be constrained *a priori*. Accordingly, we assigned the range HFR = 0.1–0.5 (Table 1) and, in parallel, we also assigned the constraint $[\text{Fe-Flow}_{4,2}/\text{Fe-Flow}_4] \leq 0.0033$ to coincide with the upper bound predicted by Sander and Koschinsky (2011). Unfortunately, a numerical consequence of imposing such small values for the ratio $[\text{Fe-Flow}_{4,2}/\text{Fe-Flow}_4]$ was that our linear inverse modeling allowed HFR to take any value within the 0.1–0.5 range and could not allow us to progress further following this approach. Accordingly we decided, instead, to use our model in a deterministic mode: i.e. to continue to set HFR values *a priori* and then explore the effects of varying that parameter on different Fe-Flows.

3.2. Fe cycling, deterministic direct approach

In the next stage of our calculations we computed the values of the different Fe-Flows by considering different HFR values, together with model Eqs. (M1) to (M5) and assuming that $[\text{Fe-Flow}_{4,2}/\text{Fe-Flow}_4]$ varied across the values 0.075, 0.04, 0.01,

Table 2

Results of deterministic direct model runs, for HFR = 0.1–0.5, assuming that $[\text{Fe-Flow}_{4,2}/\text{Fe-Flow}_4] = 0.075, 0.04, 0.01, 0.0033$ and 0.001. All reported flows represent global ocean fluxes, in kt Fe yr⁻¹. In these model runs, the values of Fe-Flow₁, Fe-Flow_{1,1}, Fe-Flow_{1,2}, Fe-Flow₂, Fe-Flow₃ and Fe-Flow₄ were the same, irrespective of changing values for $[\text{Fe-Flow}_{4,2}/\text{Fe-Flow}_4]$, and the parameter $[\text{Fe}]_2$ was held constant (0.00056 μmol kg⁻¹). The values for Fe-Flow_{4,2} (in italics) varied with corresponding values for $[\text{Fe-Flow}_{4,2}/\text{Fe-Flow}_4]$ (values labeled in parentheses in left column).

HFR	0.1	0.2	0.3	0.4	0.5
Fe-Flow ₁	503	1005	1508	2010	2513
Fe-Flow _{1,1}	251	503	754	1005	1257
Fe-Flow _{1,2}	251	503	754	1005	1257
Fe-Flow ₂	0.2	0.2	0.2	0.2	0.1
Fe-Flow ₃	0.9	2.0	3.2	4.3	5.5
Fe-Flow ₄	252	505	757	1010	1262
<i>Fe-Flow_{4,2}</i> (0.075)	19	38	57	76	94
<i>Fe-Flow_{4,2}</i> (0.04)	10	20	30	40	50
<i>Fe-Flow_{4,2}</i> (0.01)	2.5	5.0	7.6	10.1	12.6
<i>Fe-Flow_{4,2}</i> (0.0033)	0.8	1.7	2.5	3.3	4.2
<i>Fe-Flow_{4,2}</i> (0.001)	0.3	0.5	0.8	1.0	1.3

and 0.0033, and 0.001 (Table 2). The values for $[\text{Fe-Flow}_{4,2}/\text{Fe-Flow}_4]$ chosen for this effort were selected to not only include the range of values predicted from Sander and Koschinsky (2011) but also to extend the range upward so that our model would also include the higher values of 0.04 and 0.075 estimated by Bennett et al. (2008) and Hawkes et al. (2013), respectively. All simulated Fe-Flows increased with increasing HFR, with the exception of Fe-Flow₂ which decreased at HFR = 0.5 (Table 2). Fe-Flow₃ remained low for all model runs and the dominant contribution to Fe-Flow₄ was from Fe-Flow_{1,2}, indicating that most of the Fe incorporated into the non-buoyant plume was supplied from focused high-temperature venting. Importantly, however, for any values of $[\text{Fe-Flow}_{4,2}/\text{Fe-Flow}_4]$ lower than 0.01, the corresponding values of Flow_{4,2} were considerably smaller than those that had been reported previously for dissolved Fe supply to the global ocean of 50.3 kt Fe yr⁻¹ (Tagliabue et al., 2010). Indeed, even in the limit, for values of $[\text{Fe-Flow}_{4,2}/\text{Fe-Flow}_4] < 0.01$, then even if all the Fe in the focused vent flow was incorporated into the non-buoyant plume (i.e. $k = 0$ in Eq. (P1.1); Fe-Flow₁ = Fe-Flow_{1,2}), values of Flow_{4,2} would still not exceed 25 kt Fe yr⁻¹. Clearly, there was a need to parameterize our model differently.

3.3. Fe cycling, deterministic inverse approach

We explored the alternative parameterization of our model by setting $\text{Fe-Flow}_{4,2} = 229.0$ kt Fe yr⁻¹ *a priori*. This represents an updated value for the global dissolved Fe flux required to sustain worldwide dissolved Fe distributions, as re-calculated most recently in response to the 2013 US GEOTRACES expedition that has traced dissolved Fe dispersion over >4000 km away from the southern EPR at ~15° S (Sedwick et al., 2014; Resing et al., submitted for publication). As discussed earlier, values for $[\text{Fe}]_1$ and Fe-Flow₁, and for $[\text{Fe}]_3$ and Fe-Flow₃ have all been well constrained recently, through high quality observations and uncertainties for $[\text{Fe}]_2$ and Fe-Flow₂ remain the highest among the three. Accordingly, we selected $[\text{Fe}]_2$ and Fe-Flow₂ as the variables for our deterministic inverse modeling approach and used the model to estimate values for these parameters. Direct modeling Eqs. (M1), (M1.1), (M1.2), (M3), (M4), (M4.1), and (M4.2) were used to calculate the flows throughout the system and then inverse modeling Eqs. (M6) and (M7) were used to estimate $[\text{Fe}]_2$ and Fe-Flow₂, respectively. The inverse model was run using the same five values for the ratio $[\text{Fe-Flow}_{4,2}/\text{Fe-Flow}_4]$ that were used previously (Section 3.2), ranging from 0.075 to 0.001 plus an additional intermediate value of $\text{Fe-Flow}_{4,2}/\text{Fe-Flow}_4 = 0.02$. Results of our deterministic inverse model runs are presented in Table 3. To allow for

Table 3

Results of deterministic inverse model runs assuming that $\text{Fe-Flow}_{4.2} = 229.0$ kt Fe yr^{-1} (Sedwick et al., 2014; Resing et al., submitted for publication), and $[\text{Fe-Flow}_{4.2}/\text{Fe-Flow}_4] = 0.075, 0.04, 0.02, 0.01, 0.0033$ & 0.001 . All reported flows represent global ocean fluxes, in kt Fe yr^{-1} ; values for $[\text{Fe}]_2$ are in $\mu\text{mol kg}^{-1}$. In these runs, values for Fe-Flow_1 , $\text{Fe-Flow}_{1.1}$, $\text{Fe-Flow}_{1.2}$, Fe-Flow_3 , & $\text{Fe-Flow}_{4.2}$ were invariant with changing $[\text{Fe-Flow}_{4.2}/\text{Fe-Flow}_4]$ but values for Fe-Flow_4 , Fe-Flow_2 & $[\text{Fe}]_2$ (shown in italics) all varied with $[\text{Fe-Flow}_{4.2}/\text{Fe-Flow}_4]$ (values labeled in parentheses in left column).

HFR	0.1	0.2	0.3	0.4	0.5
Fe-Flow_1	503	1005	1508	2010	2513
$\text{Fe-Flow}_{1.1}$	251	503	754	1005	1257
$\text{Fe-Flow}_{1.2}$	251	503	754	1005	1257
Fe-Flow_3	1	2	3	4	5
$\text{Fe-Flow}_{4.2}$	229	229	229	229	229
<i>Fe-Flow_4 (0.075)</i>	<i>3053</i>	<i>3053</i>	<i>3053</i>	<i>3053</i>	<i>3053</i>
<i>Fe-Flow_4 (0.04)</i>	<i>5724</i>	<i>5724</i>	<i>5724</i>	<i>5724</i>	<i>5724</i>
<i>Fe-Flow_4 (0.02)</i>	<i>11,448</i>	<i>11,448</i>	<i>11,448</i>	<i>11,448</i>	<i>11,448</i>
<i>Fe-Flow_4 (0.01)</i>	<i>22,896</i>	<i>22,896</i>	<i>22,896</i>	<i>22,896</i>	<i>22,896</i>
<i>Fe-Flow_4 (0.0033)</i>	<i>69,383</i>	<i>69,383</i>	<i>69,383</i>	<i>69,383</i>	<i>69,383</i>
<i>Fe-Flow_4 (0.001)</i>	<i>228,965</i>	<i>228,965</i>	<i>228,965</i>	<i>228,965</i>	<i>228,965</i>
<i>Fe-Flow_2 (0.075)</i>	<i>2801</i>	<i>2548</i>	<i>2296</i>	<i>2043</i>	<i>1791</i>
<i>Fe-Flow_2 (0.04)</i>	<i>5472</i>	<i>5219</i>	<i>4967</i>	<i>4715</i>	<i>4462</i>
<i>Fe-Flow_2 (0.02)</i>	<i>11,196</i>	<i>10,944</i>	<i>10,691</i>	<i>10,439</i>	<i>10,186</i>
<i>Fe-Flow_2 (0.01)</i>	<i>22,644</i>	<i>22,392</i>	<i>22,139</i>	<i>21,887</i>	<i>21,634</i>
<i>Fe-Flow_2 (0.0033)</i>	<i>69,131</i>	<i>68,879</i>	<i>68,626</i>	<i>68,374</i>	<i>68,121</i>
<i>Fe-Flow_2 (0.001)</i>	<i>228,712</i>	<i>228,460</i>	<i>228,207</i>	<i>227,955</i>	<i>227,702</i>
<i>$[\text{Fe}]_2$ (0.075)</i>	<i>7</i>	<i>7</i>	<i>7</i>	<i>7</i>	<i>8</i>
<i>$[\text{Fe}]_2$ (0.04)</i>	<i>13</i>	<i>14</i>	<i>15</i>	<i>17</i>	<i>19</i>
<i>$[\text{Fe}]_2$ (0.02)</i>	<i>26</i>	<i>29</i>	<i>32</i>	<i>37</i>	<i>43</i>
<i>$[\text{Fe}]_2$ (0.01)</i>	<i>53</i>	<i>59</i>	<i>67</i>	<i>77</i>	<i>92</i>
<i>$[\text{Fe}]_2$ (0.0033)</i>	<i>163</i>	<i>182</i>	<i>208</i>	<i>241</i>	<i>289</i>
<i>$[\text{Fe}]_2$ (0.001)</i>	<i>539</i>	<i>605</i>	<i>691</i>	<i>805</i>	<i>965</i>

variability in the predicted global dissolved hydrothermal Fe flux (4.1 ± 0.3 Gmol/yr = 212.2 – 245.7 kt Fe yr^{-1} , Sedwick et al., 2014; Resing et al., submitted for publication) we have also rerun the same deterministic inverse model computations for scenarios that encompass the high and low bounds for our deterministic inverse calculations. Those results, which do not depart by more than 10% from any of the diverse values presented in Table 3, are presented in the supporting on-line material as Appendices A and B.

Comparisons between the direct (Table 2) and inverse (Table 3) deterministic modeling approaches show that there were two types of Fe-Flow in the simulations. Computed values for Fe-Flow_1 , $\text{Fe-Flow}_{1.1}$, and $\text{Fe-Flow}_{1.2}$ were identical for the direct and inverse approaches because the equations used to compute those flows do not include $[\text{Fe}]_2$, which was treated differently in the two types of approach. Conversely, Fe-Flow_2 was much higher in the inverse model runs than in the direct modeling approach (Fe-Flow_3 was negligible in both circumstances). The reason for this marked increase is because the values of $\text{Fe-Flow}_{4.2}$ (hence, also, Fe-Flow_4 and $\text{Fe-Flow}_{4.1}$) that were imposed in the inverse calculations were much higher than those that were obtained in the direct calculations, resulting in calculated values for $[\text{Fe}]_2$ (Table 3) that were 4 to 6 orders of magnitude higher than the minimum values that we had imposed in the calculations reported in Table 2. Importantly, $\text{Fe-Flow}_{1.2}$ remained small relative to Fe-Flow_2 in all values considered in our model runs (Table 3) indicating that using different values for the parameter k (Eq. (P1.1)), other than 0.5, would have had little effect on the other Fe-flows calculated.

Comparisons between results corresponding to differing values of $[\text{Fe-Flow}_{4.2}/\text{Fe-Flow}_4]$ used with the deterministic inverse approach also revealed two types of variable (Table 3). As the value for the ratio $[\text{Fe-Flow}_{4.2}/\text{Fe-Flow}_4]$ decreases, the values for all of Fe-Flow_4 , $[\text{Fe}]_2$, and Fe-Flow_2 increase. By contrast, values for Fe-Flow_1 , $\text{Fe-Flow}_{1.1}$, $\text{Fe-Flow}_{1.2}$, and Fe-Flow_3 show no response to the change in $[\text{Fe-Flow}_{4.2}/\text{Fe-Flow}_4]$. This is significant, because it indicates that the additional Fe carried by the non-buoyant

Table 4

Flux ratios ($\text{Fe-Flow}_2/\text{Fe-Flow}_4$) calculated from Table 3, corresponding to changing $[\text{Fe-Flow}_{4.2}/\text{Fe-Flow}_4]$ (values labeled in parentheses in left column).

HFR	0.1	0.2	0.3	0.4	0.5
<i>$\text{Fe-Flow}_2/\text{Fe-Flow}_4$ (0.075)</i>	<i>0.92</i>	<i>0.83</i>	<i>0.75</i>	<i>0.67</i>	<i>0.59</i>
<i>$\text{Fe-Flow}_2/\text{Fe-Flow}_4$ (0.04)</i>	<i>0.96</i>	<i>0.91</i>	<i>0.87</i>	<i>0.82</i>	<i>0.78</i>
<i>$\text{Fe-Flow}_2/\text{Fe-Flow}_4$ (0.02)</i>	<i>0.98</i>	<i>0.96</i>	<i>0.93</i>	<i>0.91</i>	<i>0.89</i>
<i>$\text{Fe-Flow}_2/\text{Fe-Flow}_4$ (0.01)</i>	<i>0.99</i>	<i>0.98</i>	<i>0.97</i>	<i>0.96</i>	<i>0.94</i>
<i>$\text{Fe-Flow}_2/\text{Fe-Flow}_4$ (0.0033)</i>	<i>1.00</i>	<i>0.99</i>	<i>0.99</i>	<i>0.99</i>	<i>0.98</i>
<i>$\text{Fe-Flow}_2/\text{Fe-Flow}_4$ (0.001)</i>	<i>1.00</i>	<i>1.00</i>	<i>1.00</i>	<i>1.00</i>	<i>1.00</i>

plume (Fe-Flow_4) when $[\text{Fe-Flow}_{4.2}/\text{Fe-Flow}_4]$ is increased must be supplied by diffuse hydrothermal Fe flow that is entrained into the buoyant plume (Fe-Flow_2). The latter accounted for >90% of Fe-Flow_4 for all values of HFR when $[\text{Fe-Flow}_{4.2}/\text{Fe-Flow}_4] < 0.02$ (Table 4).

According to our model, all considered values of $[\text{Fe-Flow}_{4.2}/\text{Fe-Flow}_4] \geq 0.0033$ (Table 3) yield predicted values for $[\text{Fe}]_2$ that fall within the broad range reported previously from field data, i.e. from 0.7 to 250 $\mu\text{mol kg}^{-1}$ (Luther et al., 2001; Koschinsky et al., 2002; Sander and Koschinsky, 2011; S. Sander, unpubl. Data). The values of 0.0033 proposed for $[\text{Fe-Flow}_{4.2}/\text{Fe-Flow}_4]$ by Sander and Koschinsky (2011) can be considered reasonable for values of HFR up to 0.4 while higher values of $[\text{Fe-Flow}_{4.2}/\text{Fe-Flow}_4]$ up to and including the 0.04 and 0.075 estimates (Bennett et al., 2008; Hawkes et al., 2013) also match to previously published literature values across the HFR range considered. By contrast, the lowest value considered, $[\text{Fe-Flow}_{4.2}/\text{Fe-Flow}_4] = 0.001$, yields predicted $[\text{Fe}]_2$ values in excess of 500 $\mu\text{mol kg}^{-1}$ which exceed the highest values ever reported in the literature (Luther et al., 2001). Accordingly, this “outlier” $[\text{Fe-Flow}_{4.2}/\text{Fe-Flow}_4]$ value was not considered further in the calculations for Corg cycling (next sections) that relied upon the outcomes from our “Fe currency” model.

In summary, our deterministic inverse modeling of Fe cycling in hydrothermal plumes allows three major inferences to be drawn:

- (1) Our model – which is based upon a global-flux value for $\text{Flow}_{4.2}$ (derived from regional-scale $\text{Fe-}^3\text{He}$ correlations) and upon a series of independently quantified concentrations and fluxes determined at and close to the seafloor at the EPR 9°50' N vent site – provides a coherent framework for investigating global-scale hydrothermal cycling which, reassuringly, yields a range of reasonable values for both HFR and $[\text{Fe}]_2$.
- (2) The range of $[\text{Fe}]_2$ calculated for all imposed $[\text{Fe-Flow}_{4.2}/\text{Fe-Flow}_4]$ values $\geq 0.33\%$ is 7–289 $\mu\text{mol kg}^{-1}$, consistent with the range of values reported previously from direct measurements of diffuse vent fluid compositions.
- (3) For all values of $[\text{Fe-Flow}_{4.2}/\text{Fe-Flow}_4] < 2.0\%$, diffuse vent flow entrained into buoyant hydrothermal plumes represents the dominant (>90%) source of Fe exported to the deep ocean via dispersing hydrothermal plumes.

3.4. Carbon cycling, DOC inputs to dispersing hydrothermal plumes

To investigate C-cycling associated with Fe in our deterministic inverse model we used the same values for water volume flux that were derived in Methods Sections 2.2.1, 2.2.2 and 2.2.3 for Water-Flow_1 , Water-Flow_2 and Water-Flow_3 , and then summed those to calculate Water-Flow_4 using the equation:

$$\text{Water-Flow}_4 = \text{Water-Flow}_1 + \text{Water-Flow}_2 + \text{Water-Flow}_3 \quad (M8)$$

To calculate the C-Flow values associated with each of these fluxes we used the parameterizations listed in Table 5, and computed the values listed in Table 6 using the family of expressions:

$$\text{C-Flow}_1 = \text{Water-Flow}_1 \times [\text{C}]_1 \quad (M8.1)$$

Table 5
Parameters used in SCOR-InterRidge WG135 hydrothermal carbon cycling calculations.

Parameter	Units	Value	Literature source
C molar mass	kg mol ⁻¹	12.000 × 10 ⁻³	—
C _{org} concentration in end-member vent-fluids	mol kg ⁻¹	16 ± 1 × 10 ⁻⁶	Values measured at Axial Volcano & Main Endeavour Field, Juan de Fuca Ridge (Lang et al., 2006).
C _{org} concentration in diffuse flow vent-fluids	mol kg ⁻¹	39–69 × 10 ⁻⁶	Values measured at Axial Volcano & Main Endeavour Field, Juan de Fuca Ridge (Lang et al., 2006).
DOC concentration in seawater	mol kg ⁻¹	38 × 10 ⁻⁶	Above & below plume values, EPR 9°50' N (Bennett et al., 2011).
C:Fe ratio in Fe-rich dispersing plume particulates	Dimensionless (mass ratio)	3.0	Value for Fe oxyhydroxide fraction of plume particulates at EPR 9°50' N (Bennett et al., 2011).

Table 6
Results of calculations for C-flow in hydrothermal plume systems. All reported flows represent global fluxes in kgCyr⁻¹; units for [C]₄ are μmol kg⁻¹. Values for all of C-Flow₂, C-Flow₄ and [C]₄ are predicted to vary as a function of varying [C]₂ values (μmol kg⁻¹, listed in parentheses in left column of table). The values for C-Flow_{4,1} are calculated as a function of changing [Fe-Flow_{4,2}/Fe-Flow₄] (values labeled in parentheses in left column).

HFR	0.1	0.2	0.3	0.4	0.5
C-Flow ₁	691,200	1,382,400	2,073,600	2,764,800	3,456,000
C-Flow ₂ (39 μmol kg ⁻¹)	3.56 × 10 ⁹	3.16 × 10 ⁹	2.77 × 10 ⁹	2.37 × 10 ⁹	1.98 × 10 ⁹
C-Flow ₂ (54 μmol kg ⁻¹)	4.93 × 10 ⁹	4.38 × 10 ⁹	3.83 × 10 ⁹	3.29 × 10 ⁹	2.74 × 10 ⁹
C-Flow ₂ (69 μmol kg ⁻¹)	6.30 × 10 ⁹	5.60 × 10 ⁹	4.90 × 10 ⁹	4.20 × 10 ⁹	3.50 × 10 ⁹
C-Flow ₃	13.0 × 10 ⁹	29.9 × 10 ⁹	46.8 × 10 ⁹	63.7 × 10 ⁹	80.6 × 10 ⁹
C-Flow ₄ (39 μmol kg ⁻¹)	16.6 × 10 ⁹	33.1 × 10 ⁹	49.6 × 10 ⁹	66.1 × 10 ⁹	82.5 × 10 ⁹
C-Flow ₄ (54 μmol kg ⁻¹)	17.9 × 10 ⁹	34.3 × 10 ⁹	50.6 × 10 ⁹	67.0 × 10 ⁹	83.3 × 10 ⁹
C-Flow ₄ (69 μmol kg ⁻¹)	19.3 × 10 ⁹	35.5 × 10 ⁹	51.7 × 10 ⁹	67.9 × 10 ⁹	84.1 × 10 ⁹
C-Flow ₄ (Seawater)	16.5 × 10 ⁹	33.0 × 10 ⁹	49.5 × 10 ⁹	66.0 × 10 ⁹	82.5 × 10 ⁹
C-Flow ₄ excess vs. seawater (39 μmol kg ⁻¹)	0.07 × 10 ⁹	0.06 × 10 ⁹	0.05 × 10 ⁹	0.04 × 10 ⁹	0.04 × 10 ⁹
C-Flow ₄ excess vs. seawater (54 μmol kg ⁻¹)	1.44 × 10 ⁹	1.28 × 10 ⁹	1.12 × 10 ⁹	0.96 × 10 ⁹	0.80 × 10 ⁹
C-Flow ₄ excess vs. seawater (69 μmol kg ⁻¹)	2.81 × 10 ⁹	2.50 × 10 ⁹	2.18 × 10 ⁹	1.87 × 10 ⁹	1.56 × 10 ⁹
[C] ₄ (39 μmol kg ⁻¹)	38.4	38.3	38.2	38.2	38.2
[C] ₄ (54 μmol kg ⁻¹)	41.5	39.7	39.1	38.8	38.6
[C] ₄ (69 μmol kg ⁻¹)	44.7	41.1	39.9	39.3	38.9
C-Flow _{4,1} (0.075)	7.8 × 10 ⁹				
C-Flow _{4,1} (0.04)	15.8 × 10 ⁹				
C-Flow _{4,1} (0.02)	33.0 × 10 ⁹				
C-Flow _{4,1} (0.01)	67.3 × 10 ⁹				
C-Flow _{4,1} (0.0033)	206.8 × 10 ⁹				

$$\text{C-Flow}_2 = \text{Water-Flow}_2 \times [\text{C}]_2 \quad (M8.2)$$

$$\text{C-Flow}_3 = \text{Water-Flow}_3 \times [\text{C}]_3 \quad (M8.3)$$

$$\text{C-Flow}_4 = \text{C-Flow}_1 + \text{C-Flow}_2 + \text{C-Flow}_3 \quad (M8.4)$$

Because the highest variability reported previously in the literature is for the parameter [C]₂, i.e. the organic carbon content of diffuse flow fluids, we have used that as the prime variable in the calculations reported in Table 6, with values of [C]₂ = 39, 54 and 69 μmol kg⁻¹ (Lang et al., 2006). The calculated values for carbon flow into the dispersing non-buoyant plume, C-Flow₄, varied primarily as a function of HFR and ranged from 16.6 to 84.1 × 10⁹ kgCyr⁻¹. Also shown in Table 6 are the predicted values of C-Flow₄ in the absence of any hydrothermal influence, assuming comparable volume fluxes of background seawater with a dissolved organic carbon (DOC) content of 38.2 μmol kg⁻¹ (Bennett et al., 2011). Subtracting these “background” values from each set of results for C-Flow₄ (presented as C-Flow₄ excess vs. seawater values in Table 6) we find that the predicted inputs of “excess” DOC to dispersing hydrothermal plumes are only 0.04–2.81 × 10⁹ kgCyr⁻¹ higher than the flows that would be predicted from comparable volume fluxes of background seawater. Further, coupling the

calculated values for C-Flow₄ with their corresponding values for Water-Flow₄ yields predicted values for the DOC content of waters entering the dispersing hydrothermal plume, [C]₄, that fall in the range 38.2–44.7 μmol kg⁻¹, in close agreement with field values from the EPR 9°50' N dispersing hydrothermal plume ([DOC] ≤ 43.2 μmol kg⁻¹, Bennett et al., 2011). Consistent with the latter work, our model predicts that DOC concentrations in waters entering hydrothermal plumes should, typically, only show 0–10% enrichment over background DOC values in the deep ocean.

3.5. Carbon cycling, POC scavenging from dispersing hydrothermal plumes

Within dispersing hydrothermal plumes, both microbial and abiotic processes may sequester dissolved organic carbon and remove it into sinking particulate matter. Indeed, close correlations have been reported previously between particulate organic carbon [POC] fluxes and the flux of Fe in the oxyhydroxide fraction of plume particulates collected in sediment traps close to the vent source at EPR 9°50' N (Bennett et al., 2011). This has allowed us to calculate a global-scale removal flux for POC associated with

Table 7

Summary of values for a range of key parameters derived from model calculations of Fe and C_{org} cycling in submarine hydrothermal plumes.

Parameter	Range	Units
Axial hydrothermal Heat-Flow Ratio (HFR) values	0.1–0.5	Dimensionless
Fraction of Fe delivered to non-buoyant plumes from hydrothermal venting that persists in dissolved form as it disperses into the ocean interior.	1.0–4.0	%
Concentration of dissolved Fe in diffuse flow, [Fe ₂] ^a	13–92	μmol kg ⁻¹
Fraction of Fe export flux derived from diffuse flow ^a	78–99	%
Predicted POC flux, from hydrothermal scavenging, that is delivered to seafloor sediments across the global deep ocean ^a	0.016–0.067	Pg C yr ⁻¹

^a For the case in which 1.0–4.0% of total vent-supplied Fe persists in dissolved form in dispersing, non-buoyant hydrothermal plumes (see *Discussion* for details).

sinking non-buoyant plume particulates by calculating Fe-Flow 4.1 from Eq. (M5), above, and then using the equation:

$$C\text{-Flow}_{4.1} = 3.0 \times \text{Fe-Flow}_{4.1} \quad (M8.5)$$

The calculated results (Table 6) are independent of HFR, but vary as a function of the value used for the ratio [Fe-Flow_{4.2}/Fe-Flow₄]. Calculated values for C-Flow_{4.1} fall in the range 7.8–206.8 × 10⁹ kg C yr⁻¹ which, importantly, indicates that the predicted removal flux for organic carbon from the ocean in association with sinking hydrothermal plume particles is significantly higher than the predicted input of excess DOC (see previous section) to those same plumes from hydrothermal vent sources.

In summary, our modeling of C cycling in hydrothermal plumes allows two major inferences to be drawn:

- (1) There is only modest, if any, enrichment to be expected in the DOC content of waters entering dispersing non-buoyant plumes directly above hydrothermal vent sites.
- (2) There should be net removal of organic carbon from dispersing hydrothermal plumes in the form of POC that settles toward the underlying seafloor in association with Fe-rich oxyhydroxide plume particles.

4. Discussion

In Table 7 we summarize our preferred values for a range of key parameters derived from our model calculations. A first important consideration is that while previously determined values of dissolved Fe concentrations in diffuse-flow fluids vary widely, from 0.7 to 250 μmol kg⁻¹ (Luther et al., 2001; Koschinsky et al., 2002), a median value in this range (20 μmol kg⁻¹, S. Sander, unpublished data) corresponds most closely to the 13–92 μmol kg⁻¹ range that would be predicted for those model runs in which [Fe-Flow_{4.2}/Fe-Flow₄] values fell in the range 1–4%. Further, from this subset of all our calculations, we would predict that entrained diffuse flow (Fe-Flow₂) should dominate the flux of Fe entering dispersing non-buoyant hydrothermal plumes (78–99%), at the global scale. Finally, while our calculated fluxes for C_{org} entering non-buoyant hydrothermal plumes are small (representing values that are only 0–10% higher than the lateral C_{org} flux from an equivalent volume of deep ocean water in the absence of any hydrothermal influence) the corresponding and much larger C_{org} removal fluxes that we calculate from dispersing hydrothermal plumes provide compelling evidence that processes active in hydrothermal plumes should not only sequester DOC from the deep ocean but may provide an important supply of POC to deep ocean sediments.

Putting our calculated values in context, our preferred range for the hydrothermally-associated carbon removal rate (0.016–0.067 Pg C yr⁻¹; Table 7) may appear to represent an extremely small flux when compared to the downward export of POC from the

sunlit upper ~200 m of the global ocean which transfers approximately 5 Pg C yr⁻¹ to the deep ocean interior (Henson et al., 2011). While the timescale for removal of most of that POC flux to depth may be rapid, and settling from the surface ocean has until now been believed to represent the primary mechanism to supply POC to the bathypelagic zone (i.e. depth-range 1000–4000 m; Honjo et al., 2008), it is also recognized that the majority of this settling flux is remineralized efficiently by prokaryotes and protists within the ocean interior, in the mesopelagic (200–1000 m) and bathypelagic zones (Aristegui et al., 2009). However, the bathypelagic zone, in particular, remains grossly under-sampled, despite representing the “master reservoir” for biologically-active carbon on Earth, and the fate of organic C in both the meso- and bathy-pelagic zones remains poorly constrained in current global carbon models (Honjo et al., 2014). Consequently, the possibility remains that while the flux of hydrothermally-associated organic C to the seafloor is extremely small compared to upper ocean POC export fluxes, it could play an important role in the deep ocean, not just locally but globally. For example, only 0.4–0.7 Pg C yr⁻¹ reaches the 2000 m depth horizon (Honjo et al., 2014). If we use the equation of Martin et al. (1987) we can predict still further attenuation of the settling POC flux such that only 55% of the organic C flux passing 2000 m should persist to more typical deep-ocean seafloor depths at 4000 m – i.e. the settling flux from photosynthetically derived POC, worldwide, should approximate to no more than 0.2–0.4 Pg C yr⁻¹. At the global scale, therefore, our model calculations suggest that hydrothermal fluxes of POC could represent 10%, and perhaps as much as 33% of the global deep ocean carbon flux arriving at the seabed. Certainly, sequestration of organic carbon into hydrothermal plume particles should dominate the delivery flux of organic matter to the deep ocean floor locally, close to mid-ocean ridges – particularly in locales such as the southern East Pacific Rise where ridge axis fluxes are highest and dispersing plumes underlie an oligotrophic upper ocean.

5. Conclusions

An internally consistent model has been developed that reconciles studies of global scale distributions of deep ocean Fe, as determined from separate modeling studies, with detailed process-oriented studies close to sites of seafloor hydrothermal venting. Further, our model predicts that dissolved Fe concentrations in diffuse hydrothermal flow, worldwide, should be of the order 10–100 μmol kg⁻¹ and that diffuse-flow hydrothermal fluxes should dominate the supply of dissolved Fe from hydrothermal systems to the deep ocean. The same model also predicts that there should be only modest, if any, water column enrichment in dissolved organic carbon that arises as a result of submarine venting. Rather, processes active in submarine hydrothermal plumes should actively sequester organic carbon from the deep ocean and

could thus play an important role, globally, in the delivery of particulate organic carbon to the underlying seafloor.

Acknowledgements

Support for this work was provided by the Scientific Committee for Ocean Research and InterRidge through joint funding of Working Group 135: Hydrothermal Energy Transfer and its Impact on Ocean Carbon Cycles (http://www.scor-int.org/Working_Groups/wg135.htm; <http://www.interridge.org/WG/carboncycles>). SCOR support was derived from grants OCE-0938349 and OCE-1243377 from the U.S. National Science Foundation, and from national SCOR committees. We enjoyed many fruitful discussions with the wider SCOR-WG135 membership prior to embarking on this project and following its inception. We are particularly indebted to our 4 reviewers and our editor whose efforts helped to significantly improve the clarity of the final manuscript. CRG acknowledges the support of NSF Grant OCE-1130870 and a Research Award from the Alexander von Humboldt foundation to prepare the final revised version of this manuscript.

Appendix. Supplementary material

Supplementary material related to this article can be found online at <http://dx.doi.org/10.1016/j.epsl.2015.03.012>.

References

- Aristegui, J., Gasol, J.M., Duarte, C.M., Herndl, G.J., 2009. Microbial oceanography of the dark ocean's pelagic realm. *Limnol. Oceanogr.* 54, 1501–1529.
- Bennett, S.A., Achterberg, E.P., Connelly, D.P., Statham, P.J., Fones, G.R., German, C.R., 2008. The distribution and stabilization of dissolved Fe in deep-sea hydrothermal plumes. *Earth Planet. Sci. Lett.* 270, 157–167.
- Bennett, S.A., Statham, P.J., Green, D.R.H., Statham, P.J., le Bris, N., McDermott, J., Prado, F., Rouxel, O.J., Von Damm, K.L., German, C.R., 2011. Dissolved and particulate organic carbon in hydrothermal plumes from the East Pacific Rise, 9°50' N. *Deep Sea Res.* 58, 922–931.
- Boyd, P.W., Ellwood, M.J., 2010. The biogeochemical cycle of iron in the ocean. *Nat. Geosci.* 3, 675–682.
- Breier, J.A., Toner, B.M., Fakra, S.C., Marcus, M.A., White, S.N., Thurnherr, A.M., German, C.R., 2012. Sulfur, sulfides, oxides and organic matter aggregated in submarine hydrothermal plumes at 9°50' N, East Pacific Rise. *Geochim. Cosmochim. Acta* 88, 216–236.
- Conway, T.M., John, S.G., 2014. Quantification of dissolved iron sources to the North Atlantic Ocean. *Nature* 511, 212–215.
- Corliss, J.B., Lyle, M., Dymond, J., 1978. The chemistry of hydrothermal mounds near the Galapagos Rift. *Earth Planet. Sci. Lett.* 40, 12–24.
- Dick, G.J., Anantharaman, K., Baker, B.J., Li, M., Reed, D.C., Sheik, C.S., 2013. The microbiology of deep-sea hydrothermal vent plumes: ecological and biogeographic linkages to seafloor and water column habitats. *Front. Microbiol.* 4, 1–16.
- Edmond, J.M., Measures, C.I., McDuff, R.E., Chan, L.H., Collier, R., Grant, B., Gordon, L.I., Corliss, J.B., 1979. Ridge crest hydrothermal activity and the balances of the major and minor elements in the ocean: the Galapagos data. *Earth Planet. Sci. Lett.* 46, 1–18.
- Elderfield, H., Schultz, A., 1996. Mid-ocean ridge hydrothermal fluxes and the chemical composition of the ocean. *Annu. Rev. Earth Planet. Sci.* 24, 191–224.
- Emerson, D., Moyer, C.L., 2002. Neutrophilic Fe-oxidizing bacteria are abundant at the Loihi Seamount hydrothermal vents and play a major role in Fe oxide deposition. *Appl. Environ. Microbiol.* 68, 3085–3093.
- Field, M.P., Sherrell, R.M., 2000. Dissolved and particulate Fe in a hydrothermal plume at 9°45' N, East Pacific Rise: slow Fe(II) oxidation kinetics in Pacific plumes. *Geochim. Cosmochim. Acta* 64, 619–628.
- Fitzsimmons, J.N., Boyle, E.A., Jenkins, W.J., 2014. Distal transport of dissolved hydrothermal iron in the deep South Pacific Ocean. *Proc. Natl. Acad. Sci.* 111, 16654–16661.
- Gartman, A., Findlay, A.J., Luther, G.W., 2014. Nanoparticulate pyrite and other nanoparticles are a widespread component of hydrothermal vent black smoker emissions. *Chem. Geol.* 366, 32–41.
- German, C.R., Campbell, A.C., Edmond, J.M., 1991. Hydrothermal scavenging at the Mid-Atlantic Ridge: modification of trace element dissolved fluxes. *Earth Planet. Sci. Lett.* 107, 101–114.
- German, C.R., Von Damm, K.L., 2003. Hydrothermal processes. In: Holland, H.D., Turekian, K.K. (Eds.), 1st Edition In: *Treatise on Geochemistry*, vol. 6, pp. 181–222.
- German, C.R., Seyfried Jr., W.E., 2014. Hydrothermal processes. In: Holland, H.D., Turekian, K.K. (Eds.), 2nd Edition In: *Treatise on Geochemistry*, vol. 8, pp. 191–233.
- Hatta, M., Measures, C.I., Wu, J., Roshan, S., Fitzsimmons, J.N., Sedwick, P., Mor-ton, P., in press. An overview of dissolved Fe and Mn distributions during the 2010–2011 U.S. GEOTRACES north Atlantic cruises: GEOTRACES GA03. *Deep Sea Res.* <http://dx.doi.org/10.1016/j.dsr.2.2014.07.005>.
- Hawkes, J.A., Connelly, D.P., Gledhill, M., Achterberg, E.P., 2013. The stabilisation and transportation of dissolved iron from high temperature vent systems. *Earth Planet. Sci. Lett.* 375, 280–290. <http://dx.doi.org/10.1016/j.epsl.2013.05.047>.
- Henson, S.A., Sanders, R., Madsen, E., Morris, P.J., Le Moigne, F., Quartly, G.D., 2011. A reduced estimate of the strength of the ocean's biological carbon pump. *Geophys. Res. Lett.* 38, L04606.
- Honjo, S., Manganini, S., Krishfield, R.A., Francois, R., 2008. Particulate organic carbon fluxes to the ocean interior and factors controlling the biological pump: a synthesis of global sediment trap programs since 1983. *Prog. Oceanogr.* 76, 217–285.
- Honjo, S., Eglinton, T.I., Taylor, C.D., Ulmer, K.M., Sievert, S.M., Bracher, A., German, C.R., Edgcomb, V., Francois, R., Iglesias-Rodriguez, M.D., van Mooy, B., Repeta, D.J., 2014. Understanding the role of the biological pump in the global carbon cycle: an imperative for ocean science. *Oceanography* 27, 10–16.
- Kadko, D., 1993. An assessment of the effect of chemical scavenging within submarine hydrothermal plumes on ocean geochemistry. *Earth Planet. Sci. Lett.* 120, 361–374.
- Klunder, M.B., Laan, P., Middag, R., de Baar, H.J.W., van Ooijen, J.C., 2011. Dissolved iron in the Southern Ocean (Atlantic sector). *Deep Sea Res.* 58, 2678–2694.
- Klunder, M.B., Laan, P., Middag, R., de Baar, H.J.W., Bakker, K., 2012. Dissolved iron in the Arctic Ocean: important role of hydrothermal sources, shelf input and scavenging removal. *J. Geophys. Res.* 117, C04014. <http://dx.doi.org/10.1029/2011JC007135>.
- Koschinsky, A., Seifert, R., Halbach, P., Bau, M., Brasse, S., De Carvalho, L.M., Fonseca, N.M., 2002. Geochemistry of diffuse low-temperature hydrothermal fluids in the North Fiji Basin. *Geochim. Cosmochim. Acta* 67, 1409–1427.
- Lang, S.Q., Butterfield, D.A., Lilley, M.D., Johnson, H.P., Hedges, J.L., 2006. Dissolved organic carbon in ridge-axis and ridge-flank hydrothermal systems. *Geochim. Cosmochim. Acta* 70, 3830–3842.
- Li, M., Toner, B.M., Baker, B.J., Breier, J.A., Sheik, C.S., Dick, G.J., 2014. Microbial iron uptake as a mechanism for dispersing iron from deep-sea hydrothermal vents. *Nat. Commun.* 5, 3192. <http://dx.doi.org/10.1038/ncomms4192>.
- Lupton, J.E., 1995. Hydrothermal plumes: near and far field. In: Humphris, S.E., Zierenberg, R.A., Mullineaux, L.S., Thomson, R.E. (Eds.), *Seafloor Hydrothermal Systems: Physical, Chemical, Biological, and Geological Interactions*. In: *Geophysical Monograph Series*, vol. 91, pp. 317–346.
- Luther III, G.W., Rozan, T.F., Taillefert, M., Nuzzio, D.B., Di Meo, C., Shank, T.M., Lutz, R.A., Cary, S.C., 2001. Chemical speciation drives hydrothermal vent ecology. *Nature* 410, 813–816.
- Martin, J.H., Knauer, G.A., Karl, D.M., Broenkow, W.W., 1987. VERTEX: carbon cycling in the northeast Pacific. *Deep Sea Res.* 34, 267–285.
- Mottl, M.J., McConachy, T.F., 1990. Chemical processes in buoyant hydrothermal plumes on the East Pacific Rise near 21° N. *Geochim. Cosmochim. Acta* 54, 1911–1927.
- Mottl, M.J., 2003. Partitioning of energy and mass fluxes between Mid-Ocean Ridge axes and flanks at high and low temperature. In: Halbach, P., Tunnicliffe, V., Hein, J. (Eds.), *Energy and Mass Transfer in Marine Hydrothermal Systems*. DUP, Berlin.
- Nielsen, S.G., Rehkämper, M., Teagle, D.A.H., Butterfield, D.A., Alt, J.C., Halliday, A.N., 2006. Hydrothermal fluid fluxes calculated from the isotopic mass balance of thallium in the ocean crust. *Earth Planet. Sci. Lett.* 251, 120–133.
- Niquil, N., Soetaert, K., Johnson, G.A., Van Oevelen, D., Bacher, C., Saint-Béat, B., Vézina, A.F., 2012. Inverse modelling in modern ecology and application to coastal ecosystems. Chapter 9.6 In: Wolanski, E., McLusky, D.S. (Eds.), *Treatise on Estuarine and Coastal Science*. In: Baird, D., Mehta, A. (Eds.), *Estuarine and Coastal Ecosystem Modelling*, vol. 9. Elsevier, Oxford.
- Nishioka, J., Obata, H., Tsumune, D., 2013. Evidence of an extensive spread of hydrothermal dissolved iron in the Indian Ocean. *Earth Planet. Sci. Lett.* 361, 26–33.
- Resing, J.A., Sedwick, P.N., German, C.R., Jenkins, W.J., Moffett, J.W., Sohst, B.M., Tagliabue, A., submitted for publication. Basin-scale transport of hydrothermal dissolved metals across the South Pacific Ocean. *Nature*.
- Rudnicki, M.D., Elderfield, H., 1993. A chemical model of the buoyant and neutrally buoyant plume above the TAG vent field, 26° N, Mid-Atlantic Ridge. *Geochim. Cosmochim. Acta* 57, 2939–2957.
- Saito, M.A., Noble, A.E., Goepfert, T.J., Lamborg, C.H., Jenkins, W.J., 2013. Slow spreading submarine ridges in the South Atlantic as a significant oceanic iron source. *Nat. Geosci.* 6, 775–779.
- Sander, S.G., Koschinsky, A., 2011. Metal flux from hydrothermal vents increased by organic complexation. *Nat. Geosci.* 4, 145–150.
- Sedwick, P.N., Resing, J.A., Sohst, B.M., Jenkins, W.J., German, C.R., Moffett, J.W., Tagliabue, A., 2014. Basin-scale transport of hydrothermal iron, manganese and aluminum across the eastern South Pacific. *EOS Trans. AGU. Abstr.* OS22B-05.

- Spiess, F.N., Macdonald, K.C., Atwater, T., Ballard, R., Carranza, A., Cordoba, D., Cox, C., Diaz-Garcia, V.M., Francheteau, J., Guerrero, J., Hawkins, J., Haymon, R., Hessler, R., Juteau, T., Kastner, M., Larson, R., Luyendyk, B., MacDougall, J.D., Miller, S., Normark, W., Orcutt, J., Rangin, C., 1980. East Pacific Rise: hot springs and geophysical experiments. *Science* 207, 1421–1433.
- Statham, P.J., German, C.R., Connelly, D.P., 2005. Iron (II) distribution and oxidation kinetics in hydrothermal plumes at the Kairei and Edmond vent sites Indian Ocean. *Earth Planet. Sci. Lett.* 263, 588–596.
- Tagliabue, A., Bopp, L., Dutay, J.C., Bowie, A.R., Chever, F., Jean-Baptiste, P., Bucciarelli, E., Lannuzel, D., Remenyi, T., Sarthou, G., Aumont, O., Gehlen, M., Jeandel, C., 2010. Hydrothermal contribution to the oceanic dissolved iron inventory. *Nat. Geosci.* 3, 252–256.
- Toner, B.M., Fakra, S.C., Manganini, S.J., Santelli, C.M., Marcus, M.A., Moffett, J.W., Rouxel, O., German, C.R., Edwards, K.J., 2009. Preservation of iron (II) by carbon-rich matrices in a hydrothermal plume. *Nat. Geosci.* 2, 197–201. <http://dx.doi.org/10.1038/NGEO433>.
- Vézina, A., Platt, T., 1988. Food web dynamics in the ocean. I. Best estimates of flow networks using inverse methods. *Mar. Ecol. Prog. Ser.* 42, 269–287.
- Wu, J., Wells, M.L., Rember, R., 2011. Dissolved iron anomaly in the deep tropical-subtropical Pacific: evidence for long-range transport of hydrothermal iron. *Geochim. Cosmochim. Acta* 75, 460–468.
- Yucel, M., Gartman, A., Chan, C.S., Luther III, G.W., 2011. Hydrothermal vents as a kinetically stable source of iron-sulphide-bearing nanoparticles to the ocean. *Nat. Geosci.* 4, 367–371.